**Acknowledgment.** We thank Drs. R. R. Chance and D. G. Peiffer for providing the P4BCMU samples, Dr. R. A. Zacher for sending us the preprints, and Prof. Z. Zhou for helpful discussions. B.C. wishes to acknowledge support of this work by the National Science Foundation Polymers Program (DMR8617820).

**Registry No.** P4BCMU (homopolymer), 68777-93-5; P4BCMU (SRU), 76135-61-0.

## References and Notes

(1) Prusik, T.; Montesalvo, M.; Wallace, T. *Radiat. Phys. Chem.* **1988**, *31*, 441.
(2) Singh, B. P.; Prasad, P. N. *J. Opt. Soc. Am. B: Opt. Phys.* **1988**, *5*, 453.
(3) Hanamura, E.; Itsubo, A. *Proc. SPIE-Int. Soc. Opt. Eng.* **1988**, *824*, 66.
(4) Patel, G. N. *Polym. Prepr.* **1978**, *19*, 154.
(5) Chu, B.; Xu, R. *Macromolcules* **1989**, *22*, 3153.
(6) Rawiso, M.; Aime, J. P.; Fave, J. L.; Schott, M.; Muller, M. A.; Schmidt, M.; Baumgartl, B.; Wegner, G. *J. Phys. Fr.* **1988**, *49*, 861.
(7) Zacher, R. Ph.D. Thesis, University of California at Santa Barbara, 1987.
(8) Peiffer, D. G., private communication.
(9) Chu, B.; Xu, R.; Maeda, T.; Dhadwal, H. S. *Rev. Sci. Instrum.* **1988**, *59*, 716.
(10) Berne, B. J.; Pecora, R. *Dynamic Light Scattering*; Wiley: New York, 1976.
(11) Koppel, D. E. *J. Chem. Phys.* **1972**, *57*, 4814.
(12) Chu, B.; Xu, R.; DiNapoli, A. *J. Colloid Interface Sci.* **1987**, *116*, 182.
(13) Xu, R.; Ford, J.; Chu, B. In *Particle Size Distribution: Assessment and Characterization*; Provder, T., Ed.; ACS Symp. Series 332; American Chemical Society: Washington, DC, 1987; pp 115-132.
(14) Newman, J.; Swinney, H. L.; Day, L. A. *J. Mol. Biol.* **1977**, *116*, 593.
(15) Tanford, C. *Physical Chemistry of Macromolecules*, Wiley: New York, 1961.
(16) Muller, M.; Schmidt, M.; Wegner, G. *Makromol. Chem., Rapid. Commun.* **1984**, *5*, 83.
(17) Chance, R. R. *Macromolecules* **1980**, *13*, 396.
(18) Aime, J. P.; Rawiso, M.; Schott, M. *Springer Ser. Solid-State Sci.* **1987**, *76*, 58.
(19) Minday, R. M.; Schmidt, L. D.; Davis, H. T. *J. Chem. Phys.* **1971**, *54*, 3112.
(20) Kitahara, A., Watanabe, A., Eds. *Electrical Phenomena at Interfaces*; Marcel Dekker: New York, 1984; p 118.
(21) Coehn, A.; Raydt, V. *Ann. Phys. (Leipzig)* **1909**, *30*, 777.
(22) Zhou, Y.; Stell, G.; Friedman, H. L. *J. Chem. Phys.* **1988**, *89*, 3836.
(23) Zacher, R. A. *J. Chem. Phys.*, in press.
(24) Lim, K. C.; Kapitulnik, A.; Zacher, R.; Heeger, A. J. *J. Chem. Phys.* **1985**, *82*, 516.
(25) Schmidt, M.; Wegner, G. *J. Chem. Phys.* **1986**, *84*, 1057.
(26) Lim, K. C.; Kapitulnik, A.; Zacher, R.; Heeger, A. J. *J. Chem. Phys.* **1986**, *84*, 1058.

# Intrinsic Dynamic Viscoelasticity of Polystyrene in Θ and Good Solvents

**Dennis W. Hair and Eric J. Amis***

*Department of Chemistry, University of Southern California, Los Angeles, California 90089-0482.* *Received February 15, 1989; Revised Manuscript Received April 22, 1989*

ABSTRACT: Intrinsic dynamic storage and loss shear moduli have been measured for polystyrene in decalin (Θ solvent) and in toluene (good solvent) with a multiple-lumped resonator instrument. The Θ-solvent data can be fit with theory by assuming fully developed hydrodynamic interaction ($h^* = 0.25$) and Gaussian coils in the Rouse-Zimm bead-spring model. For the good solvent data two treatments are used to account for the influences of chain expansion. Fitting parameters are obtained from independent measurements of radius of gyration and intrinsic viscosity. Analyses are performed with (1) the Rouse-Zimm bead-spring model with Gaussian chain statistics and reduced hydrodynamic interaction ($h^* = 0.04$), (2) a modified Rouse-Zimm model, which includes statistics of expanded chains with an independent $h^*$, and (3) a scaling type approach, which incorporates chain expansion but does not explicitly modify a draining parameter. Although we cannot discriminate between the models, the influence of chain expansion on draining is demonstrated, as is the need to find a consistent treatment.

## Introduction

Fujita has recently discussed[1] several examples of unsolved problems of polymer behavior in dilute solution. Areas of difficulty that he focused on are the magnitudes and molecular weight dependences of intrinsic viscosity, hydrodynamic factors, second virial coefficients, and the excluded-volume effect. His literature review pointed out the lack of adequate theoretical explanations, in terms of molecular parameters, for long-standing experimental results on intrinsic viscosity, radius of gyration, diffusion coefficient, sedimentation coefficient, second virial coefficient, and persistence length. For the special case of Θ conditions there is actually rather good predictive theory, but, as Fujita emphasizes, one fundamental problem that remains a key to understanding dilute solution behavior in general is the coupling between the diminution of intramolecular hydrodynamic interaction and the onset of polymer chain expansion as is precipitated by excluded-volume interactions. This coupling has previously been the subject of numerous experimental observations and theoretical treatments, particularly of intrinsic viscosity and hydrodynamic radius.[2-5]

This paper presents a new set of experimental results that illustrate this effect and require explanation. The studies are of intrinsic dynamic storage and loss shear moduli, $[G']_R$ and $[G'']_R$, of dilute flexible polymer solutions. The samples are well-characterized, nearly monodisperse, linear polystyrenes in both good solvent and Θ-solvent conditions. The data are compared to predictions from theoretical treatments that approach the problem from different sides of the hydrodynamic and excluded-volume influences.

It is well-known that the statistical radius of a polymer chain, for example, the radius of gyration, $R_G$, varies with molecular weight as $R_G \sim M^{\nu}$ where the excluded-volume

* Author to whom correspondence should be addressed.

0024-9297/89/2222-4528$01.50/0 

exponent $\nu$ reflects the transition from a non-self-avoiding random walk ($\nu = 0.5$) to a self-avoiding walk ($\nu = 0.588$). The simplest way to translate this statistical radius into consideration of the transport properties of an isolated polymer chain in solution is to model the polymer as an impermeable sphere with an effective "hydrodynamic" radius, $R_H$, which is proportional to $R_G$. One interpretation is that solvent "inside" the coil is considered to be trapped by hydrodynamic forces. To the extent that $R_H \sim R_G$, the static exponent $\nu$ will also describe hydrodynamic properties such as diffusion coefficient ($D \sim R_H^{-1} \sim M^{-\nu}$) and intrinsic viscosity ($[\eta] \sim R_G^3/M \sim M^{3\nu-1}$). For polymers in Θ conditions, $\nu = 0.5$, experimental results[1] strongly support these assignments with $D \sim M^{-0.5}$ and $[\eta] \sim M^{0.5}$.

There are also many examples, particularly with solvents of intermediate or good quality, where there is not equivalence between static and dynamic exponents.[1,6,7] These discrepancies are often observed by considering so-called universal ratios. The ratios are expected to be model independent, and the fact that they are sensitive to solvent power demonstrates that the concept of an impermeable hydrodynamic sphere is not adequate. Because of these contradictions, it is generally accepted that, as a polymer coil expands, for instance, under the influence of excluded-volume interactions, it becomes more permeable to the solvent. The lessening of the segment–segment hydrodynamic interactions, which held the solvent inside the "non-free-draining" coil, leads to partial draining for the coil and eventually to a "free-draining" coil limit. This limit is referred to as the Rouse limit and is characterized by the expectation that the friction on the polymer coil exhibits a $M^1$ dependence.

## Theory

**Gaussian Models.** The most commonly used and successful models for the dynamics of flexible polymers are based on the bead–spring model introduced by Rouse.[8] In this model, a polymer chain is constructed using $N$ beads (submolecule segments) connected by $N - 1$ spring units. A set of $N$ equations of motion are written incorporating force terms from the following: frictional drag of the solvent (treated as a continuous medium through which the perturbing external forces are transmitted to each bead); a randomizing Brownian source; and elastic spring forces, which arise from the presence and motions of the connected neighboring beads attempting to restore the molecule to its equilibrium configuration. The simplicity of the original model came in part from the assumption that the presence of a bead does not affect the velocity of the surrounding solvent and hence the velocity of the other beads. The model takes the descriptive title free-draining.

The inclusion of hydrodynamic interaction among the various beads in a chain was originally done by Zimm[9] by using the equilibrium-averaged Oseen tensor as was suggested by the Kirkwood–Riseman formalism.[10] Use of the preaveraged Oseen interaction tensor preserves the linear nature of the problem, but since the velocity of each bead now depends on the various forces acting on all of the beads in the chain, the resulting equations are more complicated. The amount of hydrodynamic interaction each bead exerts is included into the force equations by a single parameter[11] $h^*$ expressed as

$$h^* = \frac{f_o}{(12\pi^3)^{1/2}\eta_s\sigma} \tag{1}$$

where $f_o$ is the friction per bead, $\sigma$ is the size of the bead (the root-mean-square end-to-end distance of a submolecule chain), and $\eta_s$ is the solvent viscosity. The limits on hydrodynamic interaction are $h^* = 0$, corresponding to the free-draining Rouse limit, and $h^* \approx 0.25$, which is the non-free-draining limit. Although Zimm's treatment allows for varying amounts of hydrodynamic interaction, the case of full hydrodynamic interaction ($h^* = 0.25$) has become known as the Zimm limit.

When the polymer chain is perturbed, perhaps by a flow field, from its entropically favored distribution, it will relax by a mechanism that may be pictured as involving varying lengths of chain. The resulting spectrum of $N$ relaxation modes can be characterized by a set of relaxation times, $\{\tau_p\}$. The magnitude and spacing of $\{\tau_p\}$ will vary depending on the amount of hydrodynamic interaction included in the model. For the free-draining, $h^* = 0$, limit, $\{\tau_p\}$ is given by[8]

$$\tau_p = \frac{\sigma^2 f_o}{24kT \sin^2 [p\pi^2(N+1)]} \tag{2}$$

where the index $p$ signifies the relaxation mode number from 1 to $N$. In terms of measurable quantities[12]

$$\tau_p = \frac{6[\eta]\eta_s M}{\pi^2 p^2 RT} \tag{3}$$

The reduced intrinsic viscoelastic functions $[G']_R$ and $[G'']_R$ as a function of frequency $\omega$ are calculated as

$$[G']_R = \sum_{p=1}^{N} \frac{\omega^2\tau_p^2}{1+\omega^2\tau_p^2} \qquad [G'']_R = \sum_{p=1}^{N} \frac{\omega\tau_p}{1+\omega^2\tau_p^2} \tag{4}$$

and in the same form the intrinsic viscosity

$$[\eta] = \frac{RT}{M\eta_s}\sum_{p=1}^{N}\tau_p = \frac{RT\tau_1 S_1}{M\eta_s} \tag{5}$$

where $S_1$ is defined as $\sum_p \tau_p/\tau_1$. Applying eq 3 for the Rouse limit gives $S_1 = \pi^2/6$.

With hydrodynamic interaction, analytical expressions for the $\{\tau_p\}$ can only be written for chains of 2 or 3 beads. Numerical tabulations of the eigenvalues for larger chains have been compiled for specific values of $h^*$.[13] The most complete has been done by Sammler and Schrag who have also made available efficient computer programs that perform the calculations.[14] Results from calculations using the exact eigenvalues have been very successful in fitting experimental data of dynamic viscoelasticity and birefringence from polymers in Θ- and good-solvent systems.[2,12,15–20]

Nevertheless, the Rouse–Zimm formulation contains the assumption of Gaussian statistics to describe the spatial arrangement of the beads that represent the polymer molecule. While this assumption is reasonable for polymers under ideal conditions and therefore contributes to the excellent comparisons between theory ($h^* = 0.25$) and experiments in Θ solvents, the assumption is not correct for polymers with excluded volume. Even though it has been possible to match experimental results on polymers in good solvents by varying the hydrodynamic interaction with $h^*$ as an arbitrary fitting parameter,[21] the model still contains a fundamentally improper description of the chain statistics.

**Non-Gaussian Models.** Ptitsyn and Eizner[22] introduced non-Gaussian chain statistics into Zimm's theory, solving for the case of dominant hydrodynamic interaction. This work recognized that in good solvents the mean-square separation between the $i$th and $j$th bead, $\langle r_{ij}^2 \rangle$, is not a linear function of $|i - j|$ but approximately follows

a uniform expansion, writing

$$\langle r_{ij}^2 \rangle = \sigma^2 |i - j|^{1+\epsilon} \quad (6)$$

where $\epsilon$, the excluded-volume parameter, ranges from 0 in $\Theta$ condition to 0.333 in good solvent cases. Tschoegl[23] extended this approximate treatment to the case of arbitrary hydrodynamic interaction. The conclusions by these workers were that by itself the excluded-volume parameter $\epsilon$ could not account for the experimental results; an adjustable $h^*$ was also required. Even then, equally good comparisons to data were obtained by varying $h^*$ alone.[12] Other theoretical approaches to this problem have also been undertaken, which are quite sophisticated.[24] Although there has been some success in certain calculations, this has not extended to dynamic viscoelastic properties.

In a more recent investigation of the same issue, Sammler and Schrag have performed eigenvalue calculations[25] using the uniform expansion model[23] and also using a model for non-Gaussian chain configurations as obtained from renormalization group methods by Miyake and Freed.[26] From both models the effects of chain expansion on dynamic properties are comparable. Sammler and Schrag state that they expect non-free-draining behavior to correspond with Gaussian chain statistics. However, their computer experiments could not confirm this conclusion, since they treat $h^*$ and $\epsilon$ as uncoupled parameters, a situation which they acknowledge is physically unrealistic. Fits to experimental data using uniform expansion with both $h^*$ and $\epsilon$ adjustable yield $h^*$ values that are slightly higher than fits using Gaussian statistics only ($\epsilon = 0$). Sammler and Schrag were interested in extracting values of $N$ from their oscillatory flow birefringence experiment and were satisfied to note that the value of $h^*$ obtained under the approximation of Gaussian statistics "should be interpreted in the Ptitsyn–Eizner framework as a hydrodynamic interaction parameter sensitive to excluded volume effects".[25] We hope to encourage investigation of this interrelationship.

Another treatment that accounts for excluded-volume effects in modeling viscoelasticity has been advanced by Doi and Edwards.[27] Their approach is through the addition of a bead–bead potential function $U_1$

$$U_1 = \frac{v k_B T}{2} \sum_{i,j}^{N} \delta(r_i - r_j) \quad (7)$$

to the Rouse-type interaction potential

$$U = \frac{3 k_B T}{2\sigma^2} \sum_{i=2}^{N} (r_i - r_{i-1})^2 \quad (8)$$

to account for interaction between nonbonded segments. With the introduction of this potential, the Langevin equation becomes nonlinear. Through an assumption that is similar to the preaveraging assumption in the Zimm model, the problem is linearized and becomes solvable. The excluded volume again enters into the calculation of $\zeta_p$, the friction constant per segment, where a uniform expansion of the configurational distribution is applied. Following the same approach they use in the Rouse–Zimm $\Theta$ cases, Doi and Edwards obtain expressions for self-diffusion, $D_s$, rotational relaxation time, $\tau_r$, characteristic decay rate of the dynamic light-scattering structure factor, $\Gamma_k$, intrinsic viscosity, $[\eta]$, and intrinsic moduli, $[G']$, $[G'']$. For $D_s$, $\tau_r$, $\Gamma_k$, and $[\eta]$, their results are in quite good agreement with those from more detailed calculations. Their general expression for $\{\tau_p\}$ is $\tau_p = \tau_1 p^{-\mu}$ where $\mu = 2$ for Rouse model, $^3/_2$ for Zimm model with a $\Theta$ solvent, and $3\nu$ for Zimm model with a good solvent. For the intrinsic moduli, two frequency limits are given. When $\omega\tau_1 \ll 1$

$$[G'(\omega)]_R = (\omega\tau_1)^2 \sum_{p=1}^{\infty} p^{-2\mu}$$

$$[G''(\omega)]_R = \omega\tau_1 \sum_{p=1}^{\infty} p^{-\mu} \quad (9)$$

so that $[G']_R$ and $[G'']_R$ are proportional to $\omega^2$ and $\omega$, respectively. In the limit $\omega\tau_1 \gg 1$

$$[G'(\omega)]_R = (\omega\tau_1)^{1/\mu} \frac{\pi}{2\mu \sin(\pi/2\mu)}$$

$$[G''(\omega)]_R = (\omega\tau_1)^{1/\mu} \frac{\pi}{2\mu \cos(\pi/2\mu)} \quad (10)$$

which for the three limiting conditions leads to[28]

Rouse: $\mu = 2$, $\nu = ^1/_2$

$$[G']_R = 1.11(\omega\tau_1)^{1/2} \qquad [G'']_R = 1.11(\omega\tau_1)^{1/2} \quad (11)$$

Zimm, $\Theta$: $\mu = ^3/_2$, $\nu = ^1/_2$

$$[G']_R = 1.21(\omega\tau_1)^{2/3} \qquad [G'']_R = 2.09(\omega\tau_1)^{2/3} \quad (12)$$

Zimm, good: $\mu = ^9/_5$, $\nu = ^3/_5$

$$[G']_R = 1.14(\omega\tau_1)^{5/9} \qquad [G'']_R = 1.36(\omega\tau_1)^{5/9} \quad (13)$$

Note that the Rouse–Zimm $\Theta$-solvent results show frequency dependence and relative magnitudes that are exactly the same as those from the other treatments. The good-solvent result depends on the $\nu$ value, but with the Flory exponent of $^3/_5$, the frequency dependence and relative magnitude are intermediate between the results obtained in the free-draining (eq 11) and non-free-draining (eq 12) limits. Doi and Edwards make no explicit assignment for an $h^*$ parameter.

These same scaling relationships are obtained with an effective medium theory for a solution containing polymeric fractals where the fractal dimension expresses excluded volume.[29]

## Experimental Section

**Materials.** Five narrow molecular weight fractions of linear polystyrene with molecular weights $1.79 \times 10^5$ (NBS 705), $1.05 \times 10^6$ (NBS 1479), $3.75 \times 10^6$ (Toyo Soda 380), $5.50 \times 10^6$ (Toyo Soda 550), and $2.06 \times 10^7$ (Toyo Soda 2000) were used in these experiments. Each of these polymer samples (except TS380) has been used for previous studies in this laboratory.[30] The samples are of high quality with well-characterized molecular weights and low polydispersity. The TS2000 sample has a $M_w/M_n < 1.3$ while the others are 1.04–1.15 (see Table I).

The two solvents for this study, toluene (Baker) and decalin (Aldrich), were both used as received. Toluene is an extremely good solvent for PS as evidenced by the molecular weight dependence of the radius of gyration, which scales to the power $\nu = 0.596$,[30] and a Houwink–Mark–Sakurada (HMS) molecular weight exponent for intrinsic viscosity, which is $a = 0.724$ over a wide range of molecular weights.[31] At the measurement temperature of 20 °C, the viscosity of toluene is 0.5904 cP and the density 0.866 79 g/mL. The decalin as obtained was determined by gas chromatography to be 39% trans. Since the reported $\Theta$ temperatures for *cis*- or *trans*-decalin and for mixtures of decalin each vary widely,[32-35] static light scattering was used to find the actual $\Theta$ condition (second virial coefficient $A_2 = 0.0$) of $\Theta = 18.30$ °C. At this temperature decalin had a viscosity of 2.879 cP and a density of 0.891 g/mL.

**Methods.** The experimental apparatus called the Multiple Lumped Resonator (MLR) is shown in a simplified schematic in Figure 1. The fundamental design of this instrument is the same as that proposed by Birnboim[36] and developed by Schrag[37] in Ferry's laboratory at Wisconsin in the early 1970s. The resonator

**Table I**
**Polymer Samples Used in These Studies Listed with Their Molecular Weights, Polydispersities, Inverse of Intrinsic Viscosities, and Concentration Ranges Investigated**

| | | | toluene (good solvent) | | decalin (Θ solvent) | |
|---|---|---|---|---|---|---|
| sample | $M_w \times 10^6$, g mol$^{-1}$ | $M_w/M_n$ | $[\eta]^{-1}$, mg/mL | conc range, mg/mL | $[\eta]^{-1}$, mg/mL | conc range, mg/mL |
| NBS 705 | 0.179 | 1.05 | 14.7 | 0.7–34.9 | 30.70 | 7.85–26.7 |
| NBS 1479 | 1.05 | 1.1 | 4.09 | 0.1–2.0 | 12.67 | 4.30–11.3 |
| TSF 380 | 3.75 | 1.04 | 1.67 | 0.054–1.2 | | |
| TSF 550 | 5.50 | 1.15 | 1.31 | 0.051–0.97 | 5.538 | 0.797–3.85 |
| TSF 2000 | 20.6 | <1.3 | 0.474 | 0.01–0.94 | | |

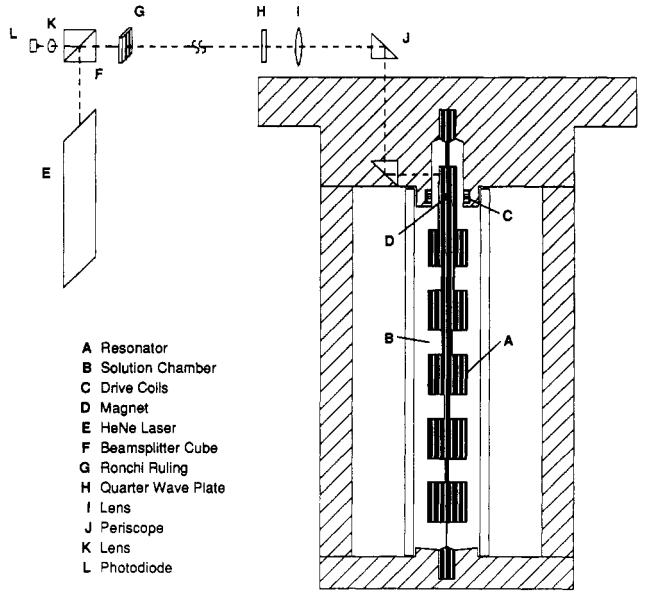


**Figure 1.** Schematic diagram of multiple-lumped resonator device. Five-lumped resonator (A) is surrounded by solvent or solution (B). It is driven into torsional resonance by current through field coils (C) acting on the permanent magnet (D) in the top extension. The beam from a HeNe laser (E) passes through a polarizing beam splitter cube (F), Ronchi ruling (G), $^1/_4$-wave retardation plate (H), lens (I), and periscope (J) before it is reflected by a mirror on the resonator. The reflected beam passes back along its path such that the image of the ruling is focused on itself. The resonator oscillation leads to a sinusoidally varying intensity transmitted through the ruling. This light is collected (K) onto a photodiode detector (L).

itself consists of a single piece of low-loss aluminum or titanium, which is machined with high precision into five inertial lumps of uniform diameter (0.795 cm) connected by torsional spring elements of specific varying diameters (0.076–0.533 cm). The inertia of each lump is equal since the bottom four lumps are identical (1.59 cm long by 0.795-cm diameter) and the top lump is 1.42 cm long with a short extension. The extension provides the means for inducing and detecting small torsional oscillations. A permanent magnet (ALNICO alloy) is precisely ground and press fit into the top extension. The extension also holds a small front surface mirror for detecting oscillations of the resonator. Five normal oscillatory modes are detected, which are four dumbbell modes with nodal points on the four spring elements and one mode where the resonator oscillates as a unit.

The resonator is clamped by its top and bottom in a rigid housing assembly, which holds it inside a precision bore glass sample chamber. The top section of the housing encloses the extension of the top resonator lump to drive and monitor the resonator oscillations. On either side of the resonator's permanent magnet are positioned small drive coils through which flows a sinusoidally oscillating current generated by a frequency synthesizer (Hewlett Packard 3325A) at particular frequencies specified to a resolution of 1 μHz. The angular displacement of the resonator is limited to less than ±0.001° and is monitored by an optical system that is based on the one used in the original MLR. This implementation uses a polarizing beam splitter, quarter-wave retarder plate, and the front surface mirror mounted at the top of the resonator extension to superimpose the image of a vertical 300 line/in. Ronchi ruling back onto the same ruling. The relative position of the ruling lines and the image lines are aligned so that as the resonator oscillates, the intensity of light passing through the optical path varies accordingly. A HeNe laser provides the light, which is detected by a fast photodiode. The advantages of the ruling image optical system are that very small angular oscillations are detected, the signal amplitude tracks the oscillation amplitude, and the frequency response is limited only by the photodetector speed.

The assembled housing is mounted in the top of a water bath, which circulates temperature-controlled water around the sample chamber. Temperature control is maintained to ±0.0005 °C (Hart Scientific Circulator 5003A) over −10 to +50 °C and is measured to ±0.02 °C accuracy and 0.000 01 °C resolution with a stabilized thermistor thermometer (Hart Scientific 1006). Special care is taken to eliminate whenever possible any mechanical vibrations that could be transmitted to the instrument. Vibrations transmitted from the circulator are reduced by controlling the water flow and by mass loading the connecting tubing. Isolation from building vibrations is provided by an air-flotation table (Newport GS-34-ST).

A sophisticated data acquisition system, which has been described in greater detail elsewhere,[37-40] is used to determine the amplitude and relative phase of the drive signal (to the field coils) and the response signal (from the photodiode detector). A powerful cross-correlation technique, combined with a dedicated 1.35-MHz add-to-memory signal averager, makes it possible to extract accurate phase and amplitude values while rejecting noise components at interfering frequencies and harmonics. The signal averager simultaneously digitizes the voltage level of the drive and response signals from the apparatus with a pair of 12-bit analog to digital converters, and it performs real time averaging to any desired extent. Typically 5000 averages are performed in 15 s. The digitized waveforms are represented as 4093 points along a single cycle of the drive and response signals. These representations are transferred to a microcomputer for cross-correlation analysis.

The amplitudes and relative phase of the drive and response signals are obtained by cross correlation. Assume two ideal signals $A$ and $B$

$$A(\omega) = A_0 \cos(\omega t + a) \qquad B(\omega) = B_0 \cos(\omega t + b) \tag{14}$$

with frequency $\omega$ and arbitrary phases $a$ and $b$. Four integrations

$$\text{I} \quad \int_0^{2\pi} A(\omega) \sin(\omega t)\, d(\omega t) = -\pi A_0 \sin a$$

$$\text{II} \quad \int_0^{2\pi} B(\omega) \sin(\omega t)\, d(\omega t) = -\pi B_0 \sin b$$

$$\text{III} \quad \int_0^{2\pi} A(\omega) \cos(\omega t)\, d(\omega t) = \pi A_0 \cos a$$

$$\text{IV} \quad \int_0^{2\pi} B(\omega) \cos(\omega t)\, d(\omega t) = \pi B_0 \cos b \tag{15}$$

are performed as summations, and the amplitudes of the signals are obtained as

$$A_0 = \frac{(\text{I}^2 + \text{III}^2)^{1/2}}{\pi} \qquad B_0 = \frac{(\text{II}^2 + \text{IV}^2)^{1/2}}{\pi} \tag{16}$$

with the phase difference $\theta \equiv |a - b|$ given by

$$\theta = \arctan(-\text{I}/\text{III}) - \arctan(-\text{II}/\text{IV}) \tag{17}$$

This method allows determination of amplitudes and relative phase with very high precision. Extensive testing of the signal

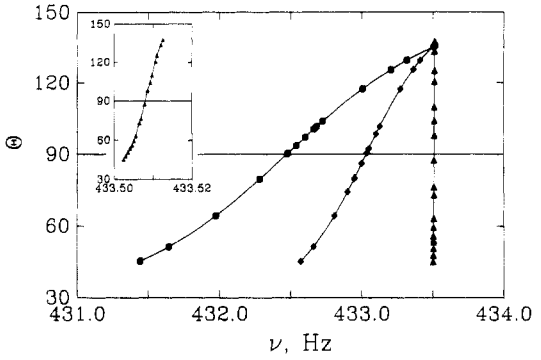


**Figure 2.** Phase difference between the resonator drive and response signals, $\theta$, plotted against frequency for the device with air (▲), solvent (◆), and polymer solution (●) in the chamber, showing a shift to lower resonance frequency as well as bandwidth broadening. The narrow bandwidth for the air curve is evident in the insert.

averager[40] has detected no systematic phase or amplitude errors between the two channels as a function of signal levels or relative phase. Reproducibility of the phase difference is better than ±0.001°.

When the resonator is driven with a signal exactly at one of its five resonance frequencies $\omega_r$, the amplitude of the response signal will be at a maximum and the relative phase of the drive and response signals will be 90°. This condition is obtained after corrections are made for constant mechanical and electronic phase errors. The bandwidth of the resonance mode is defined as the frequency difference, $\Delta\omega_B$, which shifts the phase from 45° to 135° for that particular mode. In a typical experiment $\theta$ is measured for several frequencies near resonance such that the $\theta$ vs $\omega$ response curve of the device is determined over the bandwidth region of the resonance. The insert in Figure 2 shows a representative set of $\theta$ vs $\omega$ points for the second resonance mode when the resonator is surrounded only with air. The curve is typical of an air resonance with a mechanical $Q$ for the device ($Q \equiv \omega_r/\Delta\omega_B$) on the order $10^5$ as observed for each resonance mode. This large $Q$ (for a mechanical element) contributes to the ultimate sensitivity of the device. The $\omega_r$ values are functions of temperature. For the aluminum resonator at 20 °C they are approximately 102, 433, 1065, 2565, and 6139 Hz. After the resonator frequencies and bandwidths are determined in air, the sample chamber is filled with solvent or polymer solution. Air and solvent provide calibrations of the characteristic impedance of the device. As demonstrated in Figure 2, $\Delta\omega_B$ and $\omega_r$ change drastically when solvent or solution fills the chamber.

The complex characteristic impedance of the resonator surrounded by a liquid is given by

$$Z_M^* = R_M^S + iX_M^S \tag{18}$$

where $R_M^S$ and $X_M^S$ are the surface mechanical resistance and reactance, respectively. Data to calculate $Z_M^*$ are obtained for a particular solution at each of the five resonance frequencies from such $\theta$ vs $\omega$ curves. The phase angle $\theta$ is related to $\omega$ through

$$\tan\theta = \frac{\omega[R_M^S + R_T^0]}{K[(\omega_r^0)^2 - \omega^2] - \omega X_M^S} \tag{19}$$

where $R_T^0$ describes the energy loss of the resonator in air, $\omega_r^0$ is the resonance frequency of the resonator in air, and $K$ is a geometric constant, which is proportional to the moment of inertia of the top half of the dumbbell model being considered. $R_T^0$ and $K$ are related through the air bandwidth of the resonator by

$$R_T^0 = K\Delta\omega_B \tag{20}$$

The complex characteristic impedance of the loaded resonator can be expressed in terms of the density $\rho$, and the complex shear modulus $G^*$, of the liquid

$$Z_M^* = (\rho G^*)^{1/2} = (\rho/2)^{1/2}[(G + G')^{1/2} + i(G - G')^{1/2}] \tag{21}$$

where $G^* = G' + iG''$, and $G = |G^*|$. Rearranging gives the properties of interest, the storage and loss moduli

$$G' = \frac{1}{\rho}[(R_M^S)^2 - (X_M^S)^2] \tag{22}$$

$$G'' = \frac{2}{\rho}(R_M^S)(X_M^S) \tag{23}$$

The experimental procedure is summarized as follows. First, measurements in air yield $\Delta\omega_B$ and an estimate of $\omega_r^0$. Second, measurements on a Newtonian solvent ($G' = 0$ and thus $R_M^S = X_M^S$) with a known viscosity from capillary measurements are combined with the air bandwidth to determine three calibration constants $R_T^0$, $\omega_r^0$, and $K$. With these constants in hand, $G'$ and $G''$ are calculated with eq 19 for each solution surrounding the resonator.

Each measurement with the MLR requires about 45 mL of polymer solution at a very low concentration. Stock solutions were prepared gravimetrically. For these experiments solutions were allowed to equilibrate in the dark at about 40 °C with occasional gentle swirling and inversion for 3–10 days for the toluene solutions and for 3–4 weeks for the decalin solutions. $G'$ and $G''$ were measured for each of 5–12 concentrations, with the highest typically prepared to satisfy $c[\eta] = 1$. This concentration is roughly equivalent to the chain overlap concentration $c^*$, and it is at least a factor of 3 less than the concentration that is experimentally observed to be required to see the onset of chain entanglement effects in viscosity ($\eta \sim M^{3.4}$) or viscoelasticity (the appearance of a plateau modulus).[41] Characteristics of the solution sets for the present experiments are given in Table I.

Because such low concentrations have been used, accurate $G'$ and $G''$ extrapolations to infinite dilution are permitted and these yield intrinsic moduli that can be directly compared to molecular theories for single chains. $[G']_R$ and $[G'']_R$ are obtained by the limits

$$[G']_R = \frac{M}{RT}\lim_{c\to 0}\frac{G'}{c} \qquad [G'']_R = \frac{M}{RT}\lim_{c\to 0}\frac{(G'' - \omega\eta_s)}{c} \tag{24}$$

It should be noted that, in a few cases of concentrations such that $c[\eta] > 1$, qualitative changes in the concentration dependence of the $G'$ and $G''$ extrapolations were observed. Such observations have been the subject of previous work using viscoelastic[15,42] and oscillatory flow birefringence[19] techniques. All the intrinsic moduli reported here are the result of linear extrapolations of very dilute solution data, and thus the effects of interchain interactions are removed. Extrapolations are obtained from plots of $(G'M/cRT)^{1/2}$ and $(G'' - \omega\eta_s)M/cRT$ vs $c$, as shown in Figure 3.

## Results and Discussion

The concentration range for the extrapolations shown in Figure 3 is typical. The highest concentration is about equal to the overlap concentration ($c^* = 32$ mg/mL for the case shown in Figure 3, which is the $1.05 \times 10^6$ molecular weight polymer at Θ condition), and the lowest is reduced by about 1 order of magnitude. As in the data shown, it is not unusual that the lowest concentration point for mode 5 (6139 Hz) is missing. At these concentrations, the actual values of $G'$ and $G''$ are very small, and the instrumental sensitivity is reduced at the highest frequencies. For mode 1, where the whole resonator oscillates, measurements of $G'$ as low as 0.01 dyn/cm$^2$ are possible. From the extrapolations, the error in $[G']_R$ or $[G'']_R$ is less than ±5% for each mode.

Figure 4 shows the results for three molecular weights ($1.79 \times 10^5$–$5.50 \times 10^6$) in the Θ solvent. The reduced intrinsic moduli are plotted in the traditional log format against log $\omega\tau_1$. From eq 5

$$\omega\tau_1 = \frac{\omega\eta_s[\eta]M}{RTS_1} \tag{25}$$

All of the quantities used to define $\omega\tau_1$ are known experimental values with the exception of $S_1$, which contains $\{\tau_p\}$ and is therefore model dependent. For this figure $S_1 = 2.322$ was used, which corresponds to the exact eigenvalue solution for $N = 500$ and $h^* = 0.25$. The factor $[\eta]M$

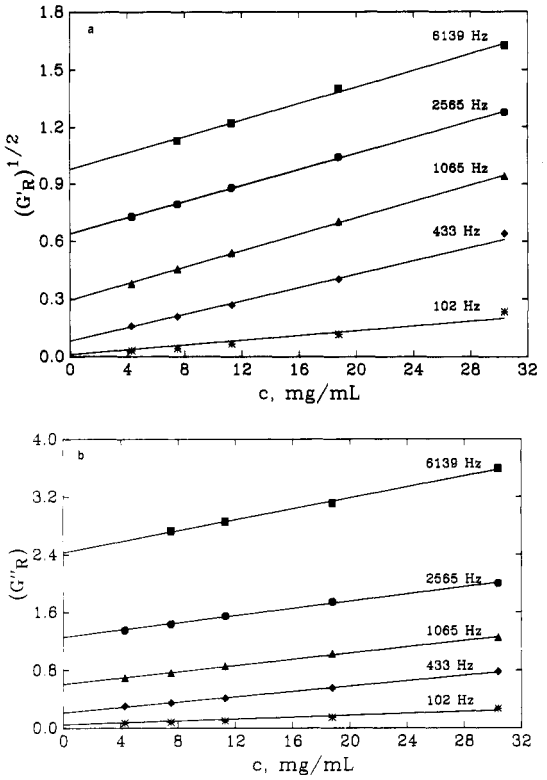


**Figure 3.** Extrapolations of $(G'_R)^{1/2}$ (a) and $G''_R$ (b) to zero concentration at each of the five resonance frequencies as indicated.

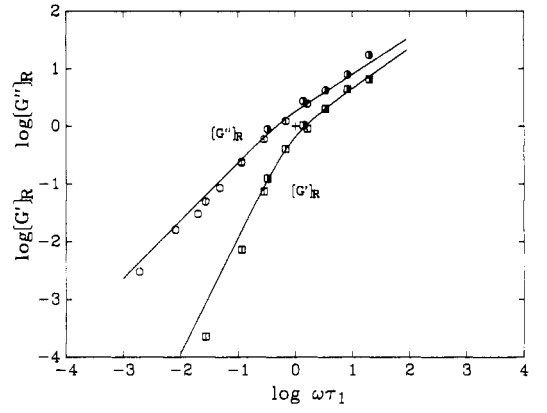


**Figure 4.** log–log plot of intrinsic storage $[G']_R$ and loss $[G'']_R$ moduli versus $\omega\tau_1$ measured in decalin at the Θ temperature (18.30 °C). Circles represent $[G'']_R$, and squares are $[G']_R$ in Figures 4, 5, and 7–9. Symbols are shaded to distinguish different molecular weights: open, $1.79 \times 10^5$; vertical line, $1.05 \times 10^6$; right half shaded $5.50 \times 10^6$. Solid curve is for Rouse–Zimm model with $h^* = 0.25$ ($N = 500$).

in eq 25 shifts data from differing molecular weights to provide nearly four decades of frequency dependence. In some previous studies, multiple solvents or temperatures have also been used (through $\eta_s$) to expand the effective frequency range. This procedure is difficult to perform while maintaining Θ conditions, and even for good-solvent conditions, it has potential to obscure effects related to specific polymer–solvent interactions. The present experiments use a single solvent and temperature for each set of data to avoid this complication. In addition the polymer–solvent systems used have been extensively studied by traditional methods such as light scattering[43-45] and viscometry[31] so that thermodynamic and hydrodynamic properties are well characterized.

There is growing concern about solvent clustering or ordering affecting the local friction on a polymer.[46] Such effects are postulated to account for anomalous high-frequency limiting viscosities.[47] It is further suggested that these effects call into question the common use of $\eta_s$ to describe the continuum in which the polymer chain exists. The primary studies of these effects have been from high-frequency dynamic viscoelastic and birefringence measurements.

On the other hand, time-resolved optical spectroscopy measurements[48] of local polymer dynamics in good and Θ solvents demonstrate no anomalous effects and can be understood by a consistent handling of solvent viscosity, solvent thermodynamic quality, temperature, and polymer molecular weight. Discrepancies regarding the influences of specific polymer–solvent interactions are far from being resolved, but in these studies they should not be a significant problem. Uses of low frequencies, low solvent viscosities, well-studied regular hydrocarbon solvents, and high molecular weight polymers combine to lead us to expect minimal, if any, anomalous "high frequency" effects.

Support for these expectations comes from comparison of Θ-solvent data with theoretical predictions of the Rouse-Zimm model with $h^* = 0.25$ as shown in Figure 4. After $h^*$ is fixed, there are no adjustable parameters in the position or shape of the curves, and therefore the agreement between data and theory for slopes and magnitudes is quite significant.

At higher frequencies the theoretical predictions will depend on the choice of $N$, the number of beads in the model. $N$ is difficult to relate precisely to molecular structure,[49] and it is argued that dependencies on $N$ are an artifact of the bead model.[50,51] Because MLR data are taken at relatively low frequency, in low viscosity solvents, and because these polymers have high molecular weights, $N$ has no effect over the experimental measurement range for any individual polymer. Assuming[20] a bead molecular weight of 5200, the $20.6 \times 10^6$ molecular weight polymer, which provides the highest effective frequencies, would have $N \approx 4000$. At MLR frequencies, changing $N$ for $N \geq 400$ causes no significant differences in $[G']_R$ and $[G'']_R$. For computational convenience $N = 500$ is used. If the experimental range was such that effects of finite chain length were significant, systematic deviations from the master curve would occur after the $[\eta]M$ effective frequency shift. Those workers who assign specific $N$ values (or equivalently bead molecular weights) for individual molecular weights must do so by fitting precise data extending to high frequencies.[20]

Moving to the results in a good solvent, the $[G']_R$ and $[G'']_R$ data for toluene solutions of five molecular weights of PS are shown in Figure 5. The abscissa does not include $S_1$ and is therefore independent of $h^*$ or other model parameters. Overlaying this data are curves corresponding to Rouse–Zimm theory with $h^* = 0.25$ (as used in Figure 5) and $h^* = 0$ (corresponding to the free-draining limit). Neither curve adequately describes the data. As anticipated, the best choice for $h^*$ appears to be between the two limits.

The value of $h^*$, which should fit the intrinsic moduli, can be predicted in a self-consistent procedure by considering the molecular weight dependence of intrinsic viscosity. This is done by calculating $[\eta]$ using eq 5 with several values of $N$ (10–700) for several specific $h^*$ values between 0 and 0.25. Slopes from plots of log $[\eta]$ vs log $N$ yield a set of HMS exponents, $a$, corresponding to the $h^*$ values, as described in the Appendix. These exponents are plotted against $h^*$ as the lower points in Figure 6. The limiting values, $a = 1$ at $h^* = 0$ and $a = 0.5$ at $h^* = 0.25$, are well-known. While Θ solution measurements experi-

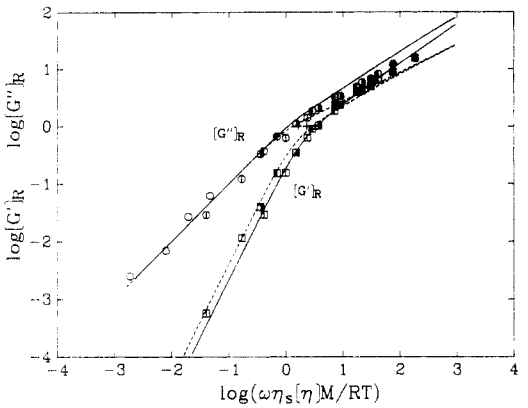


**Figure 5.** log–log plot of $[G']_R$ and $[G'']_R$ versus $\omega\tau_1 S_1$ (see text), measured in toluene at 20 °C. Different molecular weights in Figures 5 and 7–9 are indicated by: open, $1.79 \times 10^5$; vertical line, $1.05 \times 10^6$; right half shaded, $3.75 \times 10^6$; left half shaded, $5.50 \times 10^6$; solid, $20.6 \times 10^6$. Curves are from the Rouse–Zimm model: solid line, $h^* = 0.25$; dashed line, $h^* = 0$.

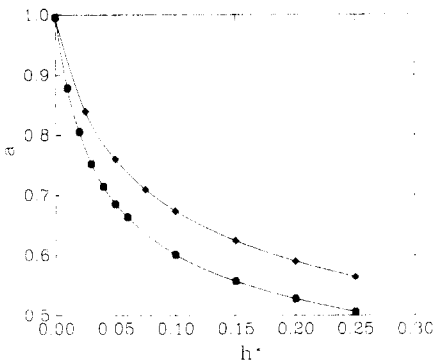


**Figure 6.** Relationship between HMS coefficient $a$ plotted versus hydrodynamic interaction parameter $h^*$. Points are generated from calculations of $[\eta]$ using the Rouse–Zimm model. Lower curve $\epsilon = 0$; upper curve $\epsilon = 0.192$.

mentally confirm $a = 0.5$ and $h^* = 0.25$, the $a = 1$ Rouse limit has not been observed. More typical values of $a = 0.55$–$0.75$ are consistent with $h^*$ of 0.03–0.16. Polystyrene in toluene at 20 °C has $a = 0.724$, which gives $h^* = 0.04$.

Figure 7 shows the good agreement of the bead–spring model ($h^* = 0.04$) with the polystyrene–toluene data. This procedure simultaneously fits the molecular weight dependence of intrinsic viscosity (over three decades of literature data follow this exponent) and the frequency-dependent dynamic viscoelasticity with a single hydrodynamic interaction parameter in the bead–spring model. As for the Θ solvent, agreement between data and theory in the magnitude and frequency dependence is significant because there are no fitting parameters once $h^*$ is specified.

Despite the satisfactory fitting of good-solvent data, it remains that the Rouse–Zimm model does not correctly include the non-Gaussian chain statistics which accompany excluded volume. Chain expansion can be modeled with eq 6 from literature values for radius of gyration[30]

$$M^{2\nu} \sim \langle R_G^2 \rangle \tag{26}$$

where $\langle R_G^2 \rangle$ is the mean-square radius of gyration for PS in toluene at 20 °C and $\nu = 0.596$. Peterlin[52] relates $\nu$, the static chain expansion, with $\epsilon$, to give $\epsilon = 0.192$. The curves in Figure 8 show the agreement of Sammler and Schrag's implementation of the uniform expansion model[25] with $\epsilon = 0.192$ and $h^* = 0.06$. The $h^*$ value was determined as described in the Appendix. Agreement with the data is very good. The significance of this result is that with the unrealistic Gaussian distribution function for chain statistics the polymer appears more free-draining. The $h^*$ value is artificially too small. The shapes of the curves in Figure 6 show that the effect on $h^*$ would be even stronger closer to Θ conditions. Often when data are compared to theory, the region very near Θ conditions is emphasized and may therefore be very sensitive to this effect.

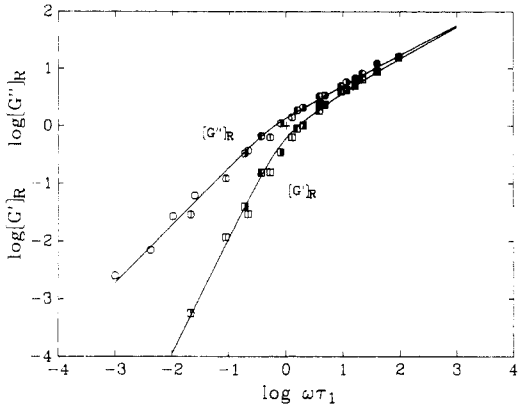


**Figure 7.** $[G']_R$ and $[G'']_R$ plotted as in Figure 5 versus $\omega\tau_1$. Curve is for the Rouse–Zimm model using $h^* = 0.04$ ($\epsilon = 0$) as determined from Figure 6.

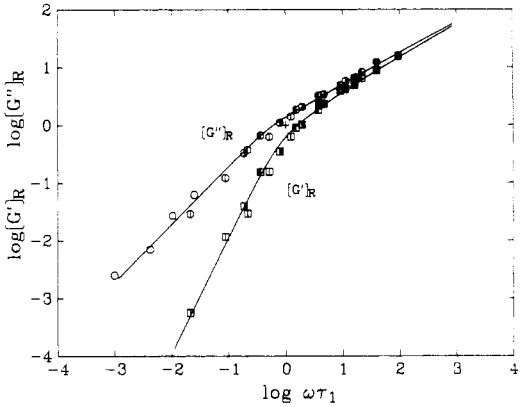


**Figure 8.** Data from Figure 7 with curve calculated using uniform expansion model, $\epsilon = 0.192$ (deduced from LS measurements) and $h^* = 0.06$ determined from upper curve of Figure 6.

As was noted in the introduction and theory sections, alternative scaling type models have been suggested previously,[27,29] which do not explicitly contain an adjustable hydrodynamic interaction parameter. These models instead depend only on the chain expansion exponent $\nu$. A disadvantage is that only the $\omega\tau_1 \ll 1$ and $\omega\tau_1 \gg 1$ limiting slopes and relative magnitudes are obtained. Equations 9 and 12 apply to the Θ-solvent system for the $\omega\tau_1 \ll 1$ and $\omega\tau_1 \gg 1$ regions, respectively, and they are in complete agreement with the data (of Figure 4) and with the exact eigenvalue calculations in these regions. Comparison of the predicted limiting slopes with PS–toluene data is shown in Figure 9 according to eq 9 and 13. The $\nu$ parameter is taken[30] (by eq 26) as 0.60. Unlike the previous comparisons using exact eigenvalue calculations, the absolute positions of these lines are not given from theory. Nevertheless, the slopes and relative magnitudes are in excellent agreement with the data. This is particularly impressive in the $\omega\tau_1 \gg 1$ region where the single parameter $\nu$, as set by independent measurements, determines the fit. The scaling argument also gives a prediction for the HMS exponent, $a = 3\nu - 1$, which for $\nu = 0.60$ yields $a = 0.80$. The literature value is 0.724. There is not general agreement about such applications of static exponents to dynamic quantities. Previous comparisons give static exponents slightly larger ($\nu_{R_G} \cong 0.6$) than corresponding

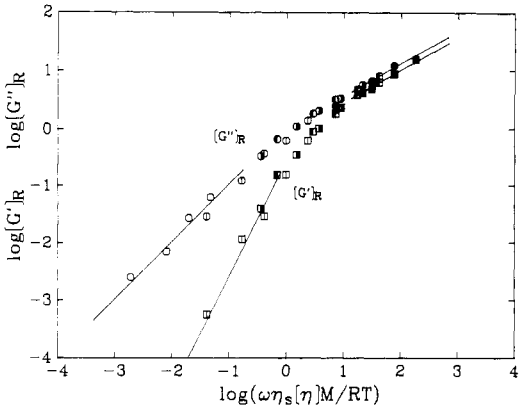


**Figure 9.** PS–toluene data are compared to slopes and relative magnitudes predicted from Doi and Edward's scaling model using $\nu = 0.596$.

dynamic values ($\nu_{R_H} \cong 0.577$),[53,54] which is consistent with these observations.

Some comparisons should be noted between the data presented here and previous work. These single-solvent Θ studies are in agreement with previous work using two different Θ solvents.[15] Over the four-decade frequency range for these experiments no solvent-specific effects are observed. In the absence of variations in thermodynamic solvent quality, viscosity alone scales chain dynamics.

For good solvents, studies with PS–toluene are consistent in that very low values of $h^*$ are observed when Gaussian chain statistics are assumed.[15] In one study with $h^* = 0$ observed, molecular weight polydispersity may have been a complicating factor.[55] Calculations by Sammler suggest this explanation.[56] In this study the polymers were all as monodisperse as are available. If polydispersity were a significant problem, a mismatching of molecular weights following the effective frequency shift would have occurred. Note that the $\omega\tau_1 \gg 1$ region, which is critical to discrimination of the chain dynamics, contains 10 pairs of points coming from three different molecular weights.

A great deal of viscoelastic and birefringence data exist[12,18,57] for PS–Aroclor solutions, and they are typically fit with $h^* = 0.15$ (Gaussian model). This result is consistent with the general expectation that Aroclor is a marginal solvent with chain dimensions near those typical of Θ chains and $\nu = 0.50$.[58] Aroclor is a common example of a solvent where specific polymer–solvent interactions probably occur. Measurements with Aroclor solutions in this lab are not nearly as extensive as published work but would also yield $h^* = 0.15$.

## Conclusions

For polystyrene in a single Θ solvent the intrinsic viscoelasticity is well described by the Rouse–Zimm model with $h^* = 0.25$. In good solvent the interpretation is not straightforward. The data are represented using the Rouse–Zimm bead–spring theory with either a Gaussian chain configuration and a low value for hydrodynamic interaction or an expanded chain model, which explicitly accounts for excluded volume and variable hydrodynamic interaction. There is also agreement with predictions of scaling methods, which include non-Gaussian chain statistics yet do not explicitly or arbitrarily modify a separate hydrodynamic interaction parameter.

Theoretical treatments for partial draining effects have recently generated new interest.[7,59,60] Most of the efforts have concentrated on hydrodynamic properties such as diffusion coefficients and intrinsic viscosity and on the acquisition of predictions of universal ratios. There remains a need for theory that consistently includes hydrodynamic interaction and excluded volume in calculations of polymer relaxation rates. Frequency-dependent viscoelastic measurements can provide tests of these theories. The results presented here should encourage more theoretical work in this area.

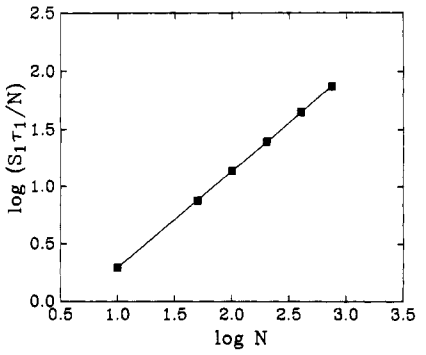


**Figure 10.** Relationship between calculated $[\eta]$ and molecular weight. $S_1\tau_1/N \sim [\eta]$ and $N \sim M$, slope gives HMS coefficient $a$.

**Acknowledgment.** We gratefully acknowledge many helpful discussions with the following people concerning experimental and theoretical aspects of this work: Drs. Robert L. Sammler, Jack F. Douglas, and Shi-Qing Wang, and Professors John D. Ferry, John L. Schrag, Timothy P. Lodge, Masao Doi, and Karl F. Freed. We are particularly indebted to Dr. Sammler and Professor Schrag for making available computer source codes, which were used extensively. This work was supported by the 3M Corp. (Nontenured Faculty Grants) and the National Science Foundation, Polymers Program (Grant DMR-8715567).

## Appendix

The dependence of intrinsic viscosity on molecular weight is given by the HMS exponent $a$. The dependence of $a$ on draining, expressed by the hydrodynamic interaction parameter $h^*$, is shown in Figure 6. This has been determined by calculations of exact eigenvalues with a bead–spring model. Figure 6 is constructed by calculating the eigenvalues at several specific values of $h^*$ between 0 and 0.25 for a series of values of $N$, the number of beads (10–700). $N$ is proportional to molecular weight, and from eq 5, $[\eta] \sim \sum(\tau_p/N) = (\tau_1 S_1/N)$. Therefore, the slope of log $(\tau_1 S_1/N)$ vs log $N$ gives $a$.

Figure 10 demonstrates the linearity of these plots. Both the ideal Gaussian model and the uniform expansion model have been calculated. Under the uniform expansion model the $i$, $j$ bead separation $\langle r_{ij}^2 \rangle = \sigma^2|i - j|^{1+\epsilon}$ where $\epsilon$ is a measure of excluded volume and is taken from light-scattering studies of radius of gyration data to be 0.192 for PS in toluene.[30] Under these models the limiting values $a = 1$ at $h^* = 0$ coincide. With Figure 6 from each model, an experimental value of $a$ can be related to a corresponding $h^*$ value. Assessment of chain draining is therefore based on intrinsic viscosity and a particular implementation of the bead–spring model, but under those contraints $h^*$ is not an arbitrary fitting parameter.

**Registry No.** Polystyrene, 9003-53-6.

## References and Notes

(1) Fujita, H. *Macromolecules* **1988**, *21*, 179.
(2) Osaki, K.; Schrag, J. L.; Ferry, J. D. *Macromolecules* **1972**, *5*, 144.
(3) Miyake, Y.; Einaga, Y.; Fujita, H.; Fukuda, M. *Macromolecules* **1980**, *13*, 588.
(4) Douglas, J. F.; Freed, K. F. *Macromolecules* **1984**, *17*, 2354.
(5) Akcasu, A. Z.; Han, C. C. *Macromolecules* **1979**, *12*, 276.
(6) Oono, Y. *J. Chem. Phys.* **1983**, *79*, 4629.

(7) Freed, K. F.; Wang, S.; Roovers, J.; Douglas, J. F. *Macromolecules* **1988**, *21*, 2219.
(8) Rouse, P. E., Jr. *J. Chem. Phys.* **1953**, *21*, 1272.
(9) Zimm, B. H. *J. Chem. Phys.* **1956**, *24*, 269.
(10) Kirkwood, J. G.; Riseman, J. *J. Chem. Phys.* **1948**, *16*, 565.
(11) Zimm[9] originally used $h = N^{1/2}f_0/(12\pi^3)^{1/2}\sigma\eta_s$. Later $h^* \equiv h/N^{1/2}$ was introduced by: Thurston, G. B.; Morrison, J. D. *Polymer* **1969**, *10*, 421.
(12) Ferry, J. D. *Viscoelastic Properties of Polymers*; John Wiley and Sons: New York, 1980; pp 183-198.
(13) Sammler, R. L.; Schrag, J. L.; Lodge, A. S. Rheology Research Center Report No. 82; University of Wisconsin—Madison: Madison, WI, 1982.
(14) Sammler, R. L.; Schrag, J. L. *Macromolecules* **1988**, *21*, 3273.
(15) Johnson, R. M.; Schrag, J. L.; Ferry, J. D. *Polym. J.* **1970**, *1*, 742.
(16) Osaki, K.; Mitsuda, Y.; Johnson, R. M.; Schrag, J. L.; Ferry, J. D. *Macromolecules* **1972**, *5*, 17.
(17) Warren, T. C.; Schrag, J. L.; Ferry, J. D. *Macromolecules* **1972**, *6*, 467.
(18) Soli, A. L.; Schrag, J. L. *Macromolecules* **1979**, *12*, 1159.
(19) Lodge, T. P.; Schrag, J. L. *Macromolecules* **1982**, *15*, 1376.
(20) Martel, C. J. T.; Lodge, T. P.; Dibbs, M. G.; Stokich, T. M.; Sammler, R. L.; Carriere, C. J.; Schrag, J. L. *Faraday Symp. Chem. Soc.* **1983**, *18*, 173.
(21) Tschoegl, N. W. *J. Chem. Phys.* **1963**, *39*, 149.
(22) Ptitsyn, O. B.; Eisner, Y. E. *Zh. Fiz. Khim.* **1958**, *32*, 2464.
(23) Tschoegl, N. W. *J. Chem. Phys.* **1964**, *40*, 473.
(24) For example: Fixman, M. *J. Chem. Phys.* **1966**, *45*, 785, 793.
(25) Sammler, R. L.; Schrag, J. L. *Macromolecules* **1989**, *22*, 3435.
(26) Miyake, A.; Freed, K. F. *Macromolecules* **1983**, *16*, 1228.
(27) Doi, M.; Edwards, S. F. *The Theory of Polymer Dynamics*; Oxford University Press: Oxford, 1986; pp 108-116.
(28) Equation 13 gives a corrected value for the $G''$ prefactor in ref 27, p 116, eq 4.167.
(29) Muthukumar, M. *J. Chem. Phys.* **1985**, *83*, 3161.
(30) Seery, T. A. P.; Shorter, J. A.; Amis, E. J. *Polymer* **1989**, *30*, 1197.
(31) Meyerhoff, G.; Appelt, B. *Macromolecules* **1979**, *12*, 968.
(32) Schulz, V. G. V.; Baumann, H. *Makromol. Chem.* **1963**, *60*, 120.
(33) Berry, G. C. *J. Chem. Phys.* **1966**, *44*, 4551.
(34) Inagaki, H.; Suzuki, H.; Fujii, M.; Matsuo, T. *J. Phys. Chem.* **1966**, *70*, 1718.
(35) Kotera, A.; Matsuda, H.; Konishi, K.; Takemura, K. *J. Polym. Sci. C* **1968**, *23*, 619.
(36) Birnboim, M. H.; Elyash, L. *J. Bull. Am. Phys. Soc.* **1966**, *11*, 165.
(37) Schrag, J. L.; Johnson, R. M. *Rev. Sci. Instrum.* **1971**, *42*, 224.
(38) Amis, E. J.; Hair, D. W. *Polym. Prepr. (Am. Chem. Soc., Div. Polym. Chem.)* **1986**, *27*, 273.
(39) Hair, D. W.; Amis, E. J. *Proc. Am. Chem. Soc., Div. Polym. Mater. Eng.* **1988**, *59*, 1121.
(40) Hair, D. W.; Niertit, F.; Hodgson, D. F.; Amis, E. J. *Rev. Sci. Instrum.* **1989**, *60*, 2780.
(41) Reference 12, p 213.
(42) Mitsuda, Y.; Schrag, L. L.; Ferry, J. D. *Polym. J.* **1973**, *4*, 668.
(43) Nose, T.; Chu, B. *Macromolecules* **1979**, *12*, 590.
(44) Nose, T.; Chu, B. *Macromolecules* **1979**, *12*, 1122.
(45) Chu, B.; Nose, T. *Macromolecules* **1980**, *13*, 122.
(46) Morris, R. L.; Amelar, S.; Lodge, T. P. *J. Chem. Phys.* **1988**, *89*, 6523.
(47) Schrag, J. L., private communication.
(48) Waldow, D. A.; Johnson, B. S.; Hyde, P. D.; Ediger, M. D.; Kitano, T.; Ito, K. *Macromolecules* **1989**, *22*, 1345.
(49) Bird, R. B.; Curtiss, C. F.; Armstrong, R. C.; Hassager, O. *Dynamics of Polymeric Liquids*; John Wiley and Sons: New York, 1987; Vol. 2, pp 76, 162.
(50) Stockmayer, W. H.; Baur, M. E. *J. Am. Chem. Soc.* **1964**, *86*, 3485.
(51) Reference 27, p 93.
(52) Peterlin, A. *J. Chem. Phys.* **1955**, *23*, 2464.
(53) Pusey, P. N.; Vaughn, J. M.; Williams, G. *J. Chem. Soc., Faraday Trans. 2* **1974**, *70*, 1969.
(54) Appelt, B.; Meyerhoff, G. *Macromolecules* **1980**, *13*, 657.
(55) Rosser, R. W.; Schrag, J. L.; Ferry, J. D. *Macromolecules* **1978**, *11*, 1060.
(56) Sammler, R. L., private communication.
(57) Lodge, T. P.; Miller, J. W.; Schrag, J. L. *J. Polym. Sci., Polym. Phys. Ed.* **1982**, *20*, 1409.
(58) Lodge, T. P.; Hermann, K. C.; Landry, M. R. *Macromolecules* **1986**, *19*, 1996.
(59) Wang, S.; Douglas, J. F.; Freed, K. F. *J. Chem. Phys.* **1987**, *87*, 1346.
(60) Shiwa, Y.; Oono, Y., submitted for publication in *J. Chem. Phys.*

# Monte Carlo Study of Ring Formation during Step-Growth Polymerization in Two Dimensions

**Allan H. Fawcett,*,† Frederick V. McBride,‡ and Jeffrey Rutherford§**

*Departments of Pure and Applied Chemistry, Computer Science, and Chemical Engineering, The Queen's University of Belfast, Northern Ireland, U.K.*
*Received February 4, 1989; Revised Manuscript Received April 24, 1989*

ABSTRACT: The formation of ring and chain molecules during an irreversible step-growth polymerization has been modeled on a two-dimensional eight-choice lattice and examined by the Monte Carlo method. No movement was allowed in the system in this study; consequently, 5.5% of the reactive groups initially present became isolated and remained unreacted, 14.1% of the monomers entered into ring molecules, and the rest became part of chain molecules. 34% of the molecules finally present were ring molecules. Mean numbers of residues in the rings and chains were obtained. The distribution function for the number of ring molecules of size $m$ had the form $R_m = A_0 m^{-\gamma}$, with $\gamma$ falling from an initial value of more than 9 to a final value of 2.7 as the degree of polymerization rose from 0.2 to 0.945.

## Introduction

The natural consequence of the nonreversible step-growth polymerization of a bifunctional monomer, if sufficient time elapses and if the monomers are in a fluid phase, is for all the material to form ring molecules. On a molecular level, at each growth stage the end group of monomer, oligomer, or polymer either reacts with an end group of a second such molecule, to form a longer chain, or reacts with the other end of the same molecule to form a ring. Rings can form provided that the simple geometrical requirement is satisfied that the two end groups of a linear molecule are adjacent to each other, but once a ring molecule has formed it cannot grow any larger (unless a bond-breaking reaction was first to open the ring and recreate end groups). Rings accumulate in number from chain molecules of the same size, but chain molecules grow in size progressively. In consequence, only small rings may form during the initial stages of the step-growth process,

† Department of Pure and Applied Chemistry.
‡ Department of Computer Science.
§ Department of Chemical Engineering.

0024-9297/89/2222-4536$01.50/0 